



# Metal/dielectric/metal sandwich film for broadband reflection reduction

Yi-Jun Jen<sup>1</sup>, Akhlesh Lakhtakia<sup>2</sup>, Meng-Jie Lin<sup>1</sup>, Wei-Hao Wang<sup>1</sup>, Huang-Ming Wu<sup>1</sup> & Hung-Sheng Liao<sup>1</sup>

<sup>1</sup>Department of Electro-Optical Engineering, National Taipei University of Technology, Taipei 106, Taiwan, <sup>2</sup>Department of Engineering Science & Mechanics, Pennsylvania State University, University Park, PA 16802, USA.

## SUBJECT AREAS:

ELECTRICAL AND  
ELECTRONIC  
ENGINEERING

PHOTONIC DEVICES

METAMATERIALS

NANOPHOTONICS AND  
PLASMONICS

Received  
18 November 2012

Accepted  
2 April 2013

Published  
17 April 2013

Correspondence and  
requests for materials  
should be addressed to  
A.L. (akhlesh@psu.  
edu)

A film comprising randomly distributed metal/dielectric/metal sandwich nanopillars with a distribution of cross-sectional diameters, displayed extremely low reflectance over the blue-to-red regime, when coated on glass and illuminated normally. When it is illuminated by normally incident light, this sandwich film (SWF) has a low extinction coefficient, its phase thickness is close to a *negative* wavelength in the blue-to-red spectral regime, and it provides weakly dispersive forward and backward impedances, so that reflected waves from the two faces of the SWF interfere destructively. Broadband reflection-reduction, over a wide range of incidence angles and regardless of the polarization state of the incident light, was observed when the SWF was deposited on polished silicon.

Reflection and transmission are two channels into which energy is redirected when a propagating electromagnetic wave encounters an interface between two dielectric materials with different refractive indices. In many applications—for example, solar cells—reflection is undesirable. Single or multilayered dielectric films are commonplace as antireflection coatings. Single-layered quarter-wave antireflection coatings with a particular refractive index and a quarter-wavelength thickness can reduce the reflection of normally incident light at a specific wavelength<sup>1</sup>. A broadband antireflection coating can be realized in theory by arranging a multilayered structure with a graded refractive-index profile from the substrate to the medium of incidence<sup>2</sup>. Nanotechnologies have recently been adopted to realize the graded refractive-index profiles by constructing subwavelength structures<sup>3,4</sup>.

A high-quality antireflection coating is necessary to enhance the absorption of light. The past ten years have seen independent extensions of relative permittivity and relative permeability of artificial isotropic materials beyond the limited ranges of those properties of naturally occurring materials. Many emerging optical applications, including optical cloaks<sup>5</sup> and flat lenses<sup>6</sup>, have been implemented to varying degrees of success, using artificial subwavelength structures with specifically designed spatial distributions of the relative permittivity  $\epsilon$  and relative permeability  $\mu$ . One goal is the development of a perfect flat lens made of isotropic negative-real-refractive-index (NRRI) materials, but loss remains a hurdle to overcome. The best available passive double-fishnet NRRI materials allow light to penetrate only to a depth around a quarter of a wavelength<sup>7</sup>. Such large losses are caused by the fact that these materials exploit material resonances. A thin film of an isotropic NRRI material with low loss is very desirable.

The optical response of a film of a bianisotropic, passive, achiral material to normally incident light can be described using an equivalent refractive index and two equivalent relative impedances<sup>8</sup>. The transmission and reflection at the interface with, say, the medium of incidence are determined by the equivalent relative impedances  $Z_+$  and  $Z_-$ , which are associated with forward (+) and backward (−) directions of light propagation. The propagation of light inside the film is determined with reference to the equivalent refractive index  $N$ .

The design of an ideal broadband antireflection coating places specific requirements on  $N$  and  $Z_{\pm}$ . Thus, the equivalent relative impedances could be required to deliver comparable amplitudes for waves reflected from both faces of the film to reach destructive interference<sup>9</sup>, with low dispersion over the antireflection spectral regime. Furthermore, the real part of  $N$  must be strongly dispersive: it must be linearly proportional to the wavelength to ensure that the optical thickness of the film remains at a constant phase thickness for all free-space wavelengths  $\lambda$  in the antireflection spectral regime.

Recently, we reported<sup>10–12</sup> the fabrication of a silver (Ag)-silicon dioxide (SiO<sub>2</sub>)-silver (Ag) sandwich film (SWF) comprising upright nanopillars by the oblique-angle-deposition (OAD) technique<sup>13,14</sup>. For normal incidence in the blue-to-red spectral regime, the SWF was found to display an equivalent refractive index with a negative real part. During further experimentation with different SWFs, we noticed that such SWFs could display very low reflectances.



That observation motivated us to deposit an SWF that would be very dark over the visible regime and over a broad range of angles of incidence. We report the morphology and optical characterization of the darkest SWF fabricated by us.

When this SWF was deposited on a glass slide, normally incident light in the blue-to-red spectral regime was almost totally transmitted into the glass slide. Analysis of measured reflection and transmission coefficients of the SWF showed that it presents a negative-real equivalent permittivity as well as a negative-real equivalent permeability—and, therefore, a negative-real equivalent refractive index—to normally incident light. In other words, the SWF performs as an isotropic NRRI material. When the same SWF was deposited on a polished amorphous-silicon wafer, the shine was taken off the silicon surface—which began to look like a dark material—thereby indicating very high absorptance over the visible regime.

Analysis showed that the first-order reflected wave at the air/SWF interface and the second-order reflected wave (that had been reflected back from the SWF/air interface) at the same interface interfere destructively regardless of the wavelength, and the linear variation of the real part of the equivalent refractive index with the free-space wavelength  $\lambda$  keeps the phase thickness of the SWF almost independent of  $\lambda$ . Our work thus offers a new modality for broadband reflection reduction.

## Results

**SWF morphology.** Figures 1(a) and (b), respectively, present the top-surface and cross-sectional images of the SWF on a scanning electron microscope (SEM). The cross-sectional image shows that each nanopillar is actually an Al-SiO<sub>2</sub>-Al sandwich. When the SWF is illuminated from the top, a magnetic reversal effect<sup>16</sup> is expected to occur in the SiO<sub>2</sub> spacer between the two Al sections of each nanopillar. The top-surface image shows that the cross-section of each nanopillar is roughly circular with diameter  $D$ . The SEM image of a single nanopillar in Fig. 1(c) provides verification of its sandwich morphology.

The histogram in Fig. 1(d) reveals that the distribution of  $D$  is Gaussian, centered at 170 nm. As the SWF is an aperiodic and irregular array of nanopillars with a distribution of cross-sectional diameters, it is expected to display broadband performance. Furthermore, the roughly circular cross-section indicates the transverse morphological isotropy of the SWF, which should make the SWF insensitive to the polarization state of normally incident light<sup>13</sup>.

**Optical Characterization of SWF-coated Glass Slide at Normal Incidence.** For optical characterization, let us assume that the  $x$  and  $y$  axes of a Cartesian coordinate system are tangential to the substrate plane, as indicated by Fig. 1, whereas the  $z$  axis is parallel to the upright Al/SiO<sub>2</sub>/Al nanopillars in the SWF. The SWF can be considered as a material continuum that presents (i) an equivalent refractive index  $N_x = N'_x + iN''_x$  and equivalent relative impedances  $Z_{\pm x} = Z'_{\pm x} + iZ''_{\pm x}$  to normally incident light whose electric field is polarized along the  $x$  axis, and (ii) refractive index  $N_y = N'_y + iN''_y$  and

equivalent relative impedances  $Z_{\pm y} = Z'_{\pm y} + iZ''_{\pm y}$  when that electric field is polarized along the  $y$  axis<sup>8</sup>. We use the qualifier *equivalent* to denote the constitution of a homogeneous film with the same reflection and transmission coefficients for normal incidence as that of the SWF under examination<sup>15,16</sup>. Despite the non-uniqueness inherent in their determination (even though we ensured the satisfaction of certain reasonable constraints<sup>12</sup>), these equivalent parameters help understand and explain the reflection and transmission characteristics for normal-incidence conditions.

The transmittance  $T_j$ , reflectance  $R_j$ , and absorptance  $A_j = 1 - (R_j + T_j)$ ,  $j \in (x, y)$ , of the SWF (deposited on BK7 glass) depend on the orientation of the electric field of the normally incident light. Figure 2(a) presents the measured spectra of  $T_j$ ,  $R_j$ , and  $A_j$ ,  $j \in (x, y)$ , of the SWF for normally incident light at  $\lambda \in \{400, 700\}$  nm. All of these quantities are expressed as percentages. The two transmittances,  $T_x$  and  $T_y$ , differ from each other by less than 3.84%, confirming the transverse isotropy of the SWF. The average transmittance  $T = (T_x + T_y)/2$  increases from 18.1% to 57.6% as  $\lambda$  increases from 400 nm to 700 nm. Both reflectances,  $R_x$  and  $R_y$ , are also virtually indistinguishable from each other, in accord with the transverse isotropy of the SWF. The average reflectance  $R = (R_x + R_y)/2$  is small and lies within the range between 0.167% and 0.968% for  $\lambda \in \{400, 700\}$  nm. The magnified spectrum of  $R$  is shown in Fig. 2(b).

The complex-valued reflection coefficients  $r_j$  and transmission coefficients  $t_j$  of the same SWF also depend on the orientation of the electric field of the normally incident light;  $R_j = |r_j|^2$  and  $T_j = N_s |t_j|^2$ , where  $N_s$  is the refractive index of the glass slide. From measurements of  $r_j$  and  $t_j$ , the quantities  $N_j$ ,  $Z_{+j}$ , and  $Z_{-j}$  were obtained at  $\lambda \in \{476, 514, 568, 647, 676\}$  nm, using a technique described elsewhere<sup>8,17</sup>. Thus, the blue-to-red spectral regime was covered.

Not surprisingly in view of the transverse morphological isotropy of the SWF, we obtained  $r_x \cong r_y$  and  $t_x \cong t_y$ , so that  $N_x \cong N_y = N$  and  $Z_{\pm x} \cong Z_{\pm y} = Z_{\pm}$ . Figure 3 presents  $N$ ,  $Z_+$ , and  $Z_-$  for the chosen five wavelengths.

The real part  $N'$  of  $N$  is negative and its magnitude increases almost linearly from  $-0.9606$  at  $\lambda = 476$  nm to  $-1.4004$  at  $\lambda = 647$  nm, and then decreases to  $-1.1998$  at  $\lambda = 676$  nm. The imaginary part  $N''$  of  $N$  is small and positive ( $\sim 0.07$ ) in the same spectral regime. Furthermore, the linearly dispersive  $N$  is accompanied by weakly dispersive  $Z_+$  and  $Z_-$ . The real part of  $Z_+$  varies between 0.9047 and 1.3870, and its imaginary part between  $-0.3063$  and  $0.2469$ . The real part of  $Z_-$  hovers around 0.2391 and 0.5637, and its imaginary part hovers between  $-0.2347$  and  $0.1493$ . The figure of merit  $FOM = -N'/N''$  exceeds 11.42 over whole spectrum of interest, and its maximum recorded value is 54.43 (at  $\lambda = 676$  nm). With a low extinction coefficient  $N''$  and a high FOM, the SWF is equivalent to a non-reflecting NRRI metamaterial for normal illumination in the blue-to-red spectral regime.

From the retrieved values of the equivalent refractive index and relative impedances, the effect of the SWF can be understood by

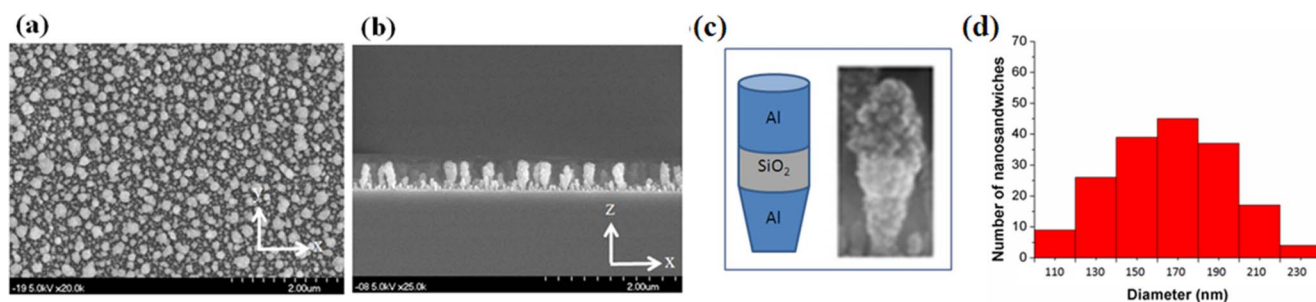


**Figure 1** | (a) Top-surface and (b) cross-sectional SEM images of the SWF of nominal thickness 480 nm. (c) Schematic and cross-sectional SEM image of a single nanopillar. (d) Histogram of diameter  $D$  in a selected  $5 \mu\text{m} \times 3 \mu\text{m}$  area on the top surface of the SWF.

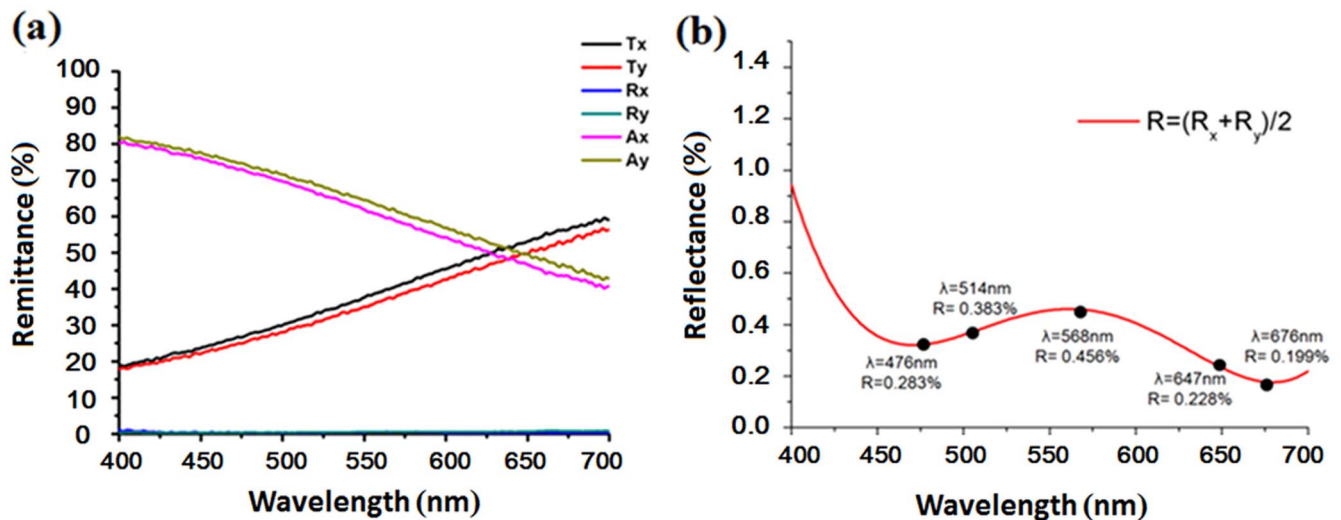


Figure 2 | Measured spectra of the transmittances, reflectances, and absorptances of the SWF on a glass slide.

tracing the propagation of light through it. For example, as shown in Fig. 4, when the SWF is normally illuminated by light with an electric field amplitude of unity and a wavelength of 647 nm, light penetrates the top interface of the SWF with transmission coefficient  $1.073 \angle -7.33^\circ$ . The first-order reflected wave has an amplitude  $r_a = 0.151 \angle -64.84^\circ$ . From the top interface to the bottom interface, the wave

propagates with a phase change of  $-14^\circ$  and the field amplitude decays to  $0.827 \angle -21.33^\circ$ . The reflection coefficient and transmission coefficient at the bottom interface are  $0.119 \angle -170.18^\circ$  and  $0.881 \angle 1.3^\circ$ , respectively. The electric field of the transmitted wave has an amplitude of  $0.729 \angle -20.03^\circ$ . The reflected wave from the bottom interface is backward-propagating with an initial field

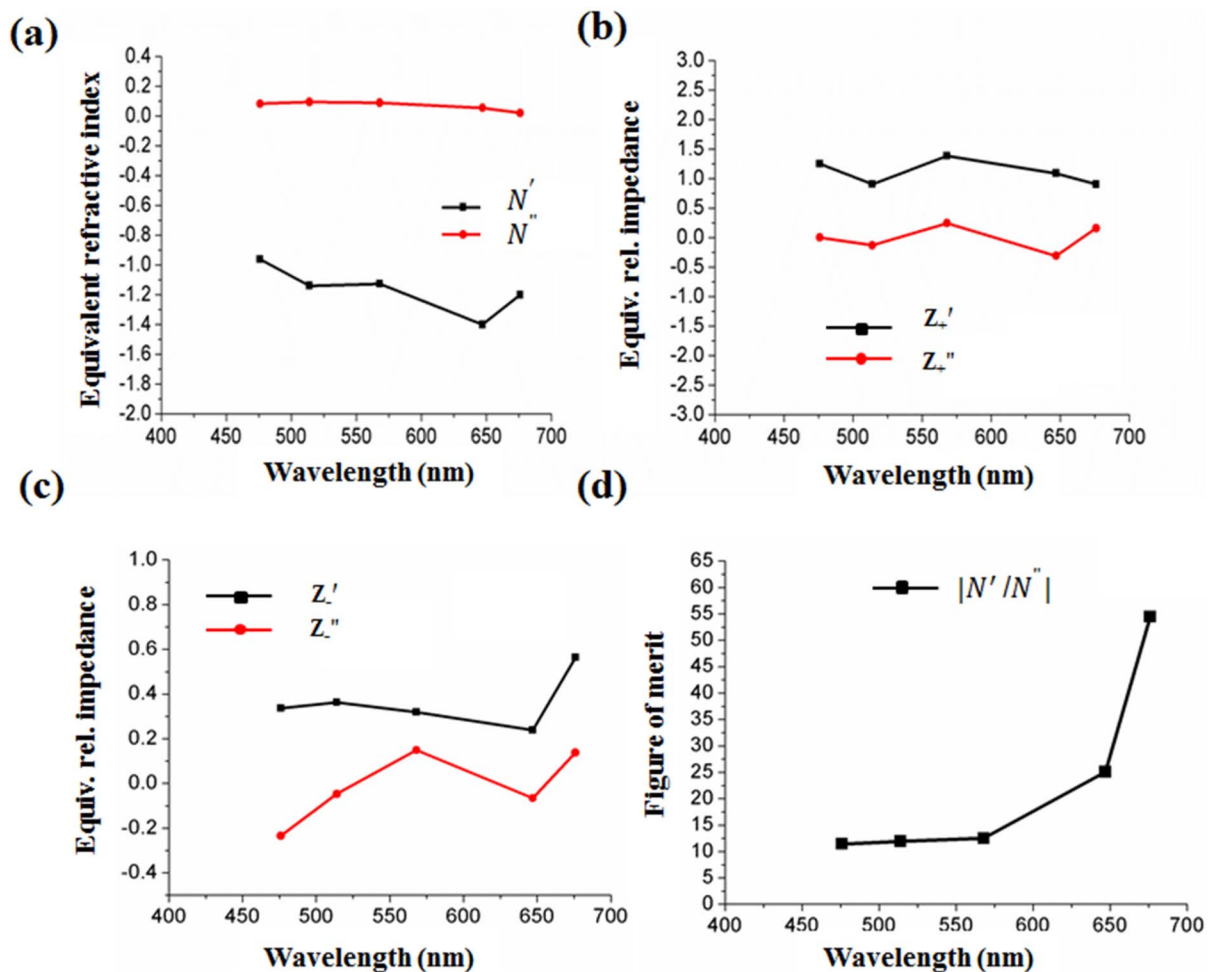
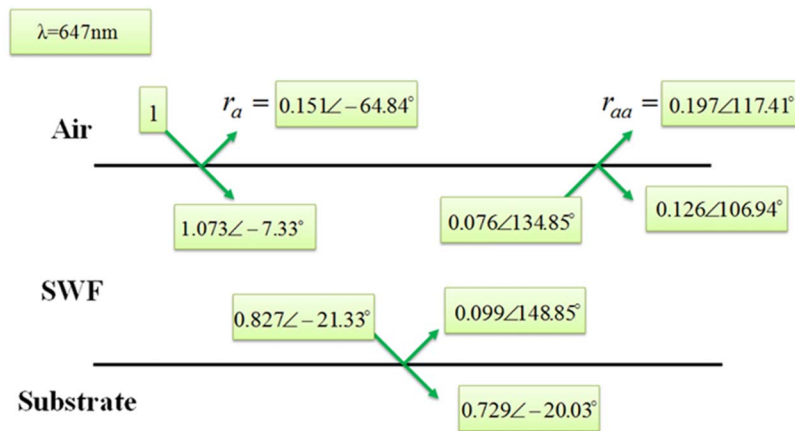


Figure 3 | Measured spectra of the real and imaginary parts of  $N$ ,  $Z_+$ ,  $Z_-$ , and the FOM, of the SWF.



**Figure 4** | Wave tracing for the SWF normally illuminated by light with an electric field amplitude of unity at wavelength of 647 nm.

amplitude of  $0.099 \angle 148.85^\circ$ . When the reflected wave returns to the top interface, the transmitted wave is the second-order reflected wave with an amplitude  $r_{aa} = 0.197 \angle 117.41^\circ$  interferes destructively with the first-order reflected wave. The reflected wave from the top interface has an initial magnitude of  $0.126 \angle -106.94^\circ$ , decaying to  $0.097 \angle 92.94^\circ$  when the wave again reaches the bottom interface. The first-order transmitted wave contributes most to the transmittance. The negative phase change indicates that backward wave propagation—characteristic of NRRI metamaterials—occurs in the SWF.

The first-order reflected wave ( $r_a$ ) and second-order reflected wave ( $r_{aa}$ ) are depicted in Fig. 5 on the complex plane to show the destructive interference at each wavelength. The low extinction coefficient  $N''$  allows the wave reflected from the SWF/glass interface to destructively interfere with the wave reflected from the air/SWF interface. Since the equivalent relative impedances vary weakly with wavelength, the phase thickness  $N'd$  can satisfy the condition of destructive interference over the blue-to-red regime in order to achieve broadband low reflectance. For  $\lambda \in [476, 676]$  nm,  $N'$  varies so that  $N'd$  lies in the range  $(-1.06 \pm 0.07)\lambda$ , quite close to  $-\lambda$ , as shown in Fig. 6. In other words, the SWF is a negative wavelength in thickness, almost independent of  $\lambda$ . Hence,

the average reflectance  $R$  of the SWF does not exceed 1% for normal incidence in a broad spectral regime.

**Oblique incidence on SWF-coated silicon wafer.** Next, we experimentally ascertained the reflectance and absorptance spectra of an SWF-coated, 0.8-mm-thick, polished wafer of amorphous silicon. A bare wafer is opaque in the visible regime. Regardless of the angle of incidence  $\theta \in [0^\circ, 90^\circ]$  with respect to the  $z$  axis as well as the linear polarization state ( $p$ - or  $s$ -polarization states), the transmittance is vanishingly small so that the sum of absorptance and reflectance equals unity.

Figure 7 shows the measured reflectances,  $R_p$  and  $R_s$ , as functions of  $\lambda \in [400, 700]$  nm and  $\theta \in [0^\circ, 60^\circ]$ , for the two linear polarization states. Clearly, the bare wafer reflects  $s$ -polarized light quite well, especially as the angle of incidence increases. Because of the display of the pseudo-Brewster phenomenon, the reflectance of  $p$ -polarized light decreases as  $\theta$  increases; although we could not make measurements at sufficiently large angles of incidence due to the limitations of our instruments, this reflectance is expected to drop to a minimum and then increase<sup>18</sup>.

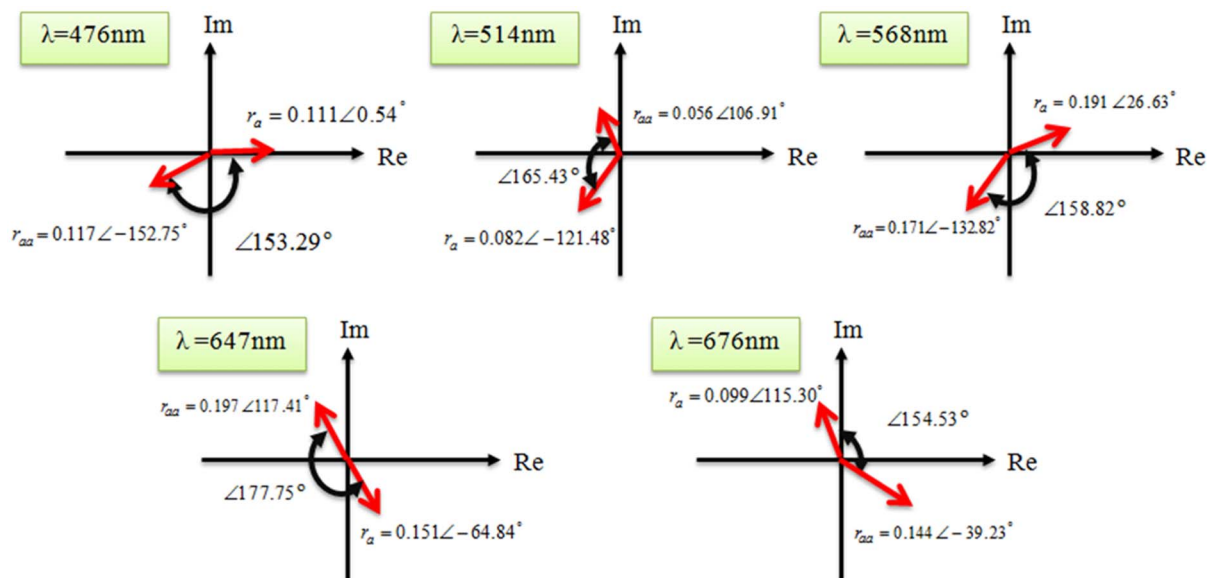


**Figure 5** | Destructive interference of first-order reflected wave of amplitude  $r_a$  and the second-order reflected wave of amplitude  $r_{aa}$  in the complex plane.



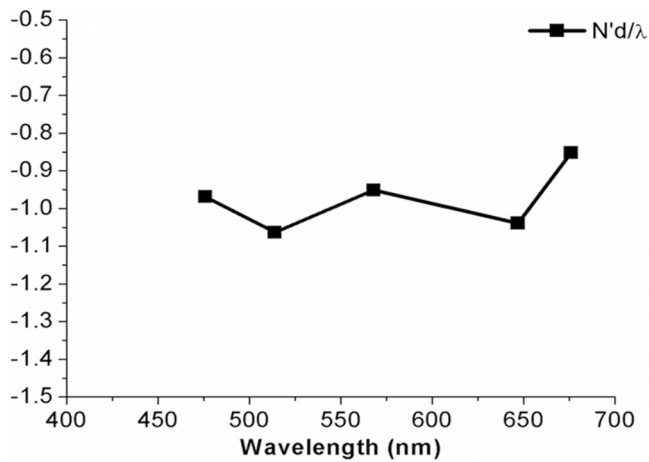


Figure 6 | Spectrum of the phase thickness  $N'd$  of the SWF.

Furthermore, the isotropy of silicon implies that rotation of the bare wafer about the  $z$  axis would not change the reflectance, a fact that we experimentally verified. When the SWF-coated wafer was rotated about the  $z$  axis from  $0^\circ$  to  $90^\circ$ , the variation of the measured reflectance was less than  $\pm 1.42\%$  from its mean value, regardless of the linear polarization state of the incident light.

The aforementioned characteristics changed dramatically when the silicon wafer was coated with the SWF. The bright reflective surface of the wafer darkened spectacularly after deposition of the SWF, as shown in the left panel of Fig. 8. The right panel of the same figure shows the measured spectra of the average reflectance  $R = (R_p + R_s)/2$  and the average absorbance  $A = 1 - R$  of the SWF-coated silicon wafer for  $\theta = 5^\circ$ , the transmittances for both linear polarization states being vanishingly small. Over the blue-to-red spectral regime, the average reflectance does not exceed  $0.82\%$ , i.e., the average absorbance remains over  $99.1\%$ . For  $\lambda \in [441, 565]$  nm, the reflectance is ultralow ( $<1\%$ ), as shown in the inset. Finally, rotation of the SWF-coated wafer about the  $z$  axis was found to not affect  $R_p$  and  $R_s$  by more than  $\pm 0.58\%$ , which reaffirmed the transverse isotropy of the SWF.

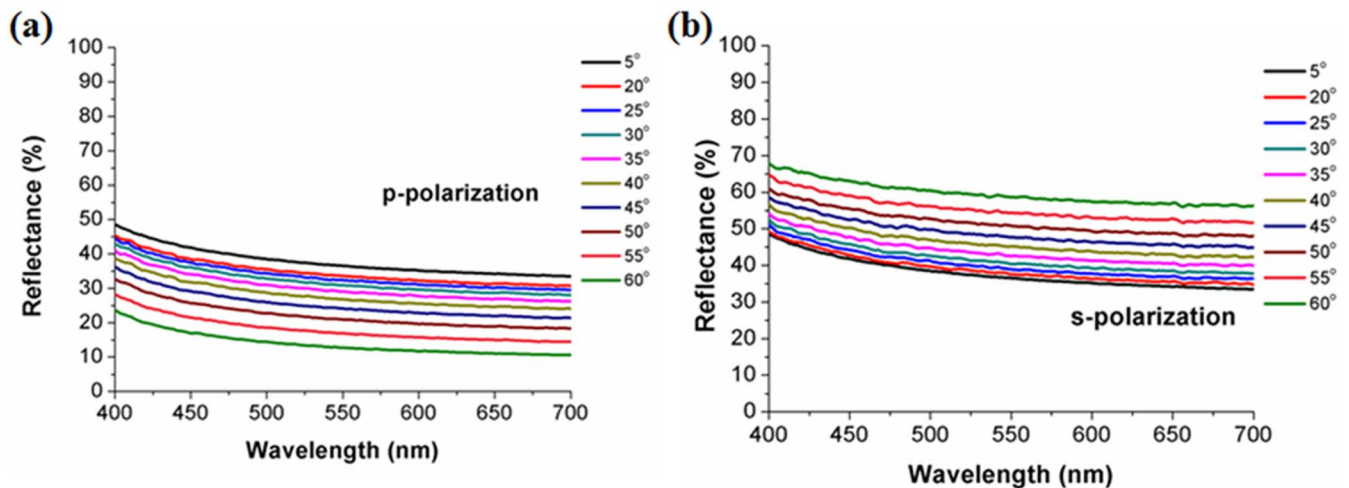


Figure 7 | Measured spectra of the reflectances of a 0.8-mm-thick bare silicon wafer, for p- or s-polarized light incident at angle  $\theta \in [0^\circ, 60^\circ]$  with respect to the  $z$  axis.

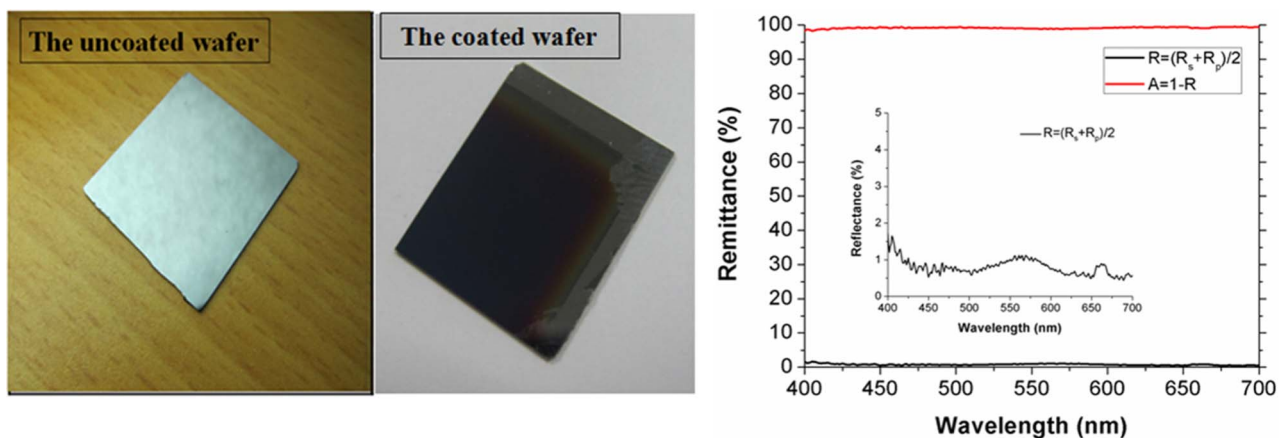
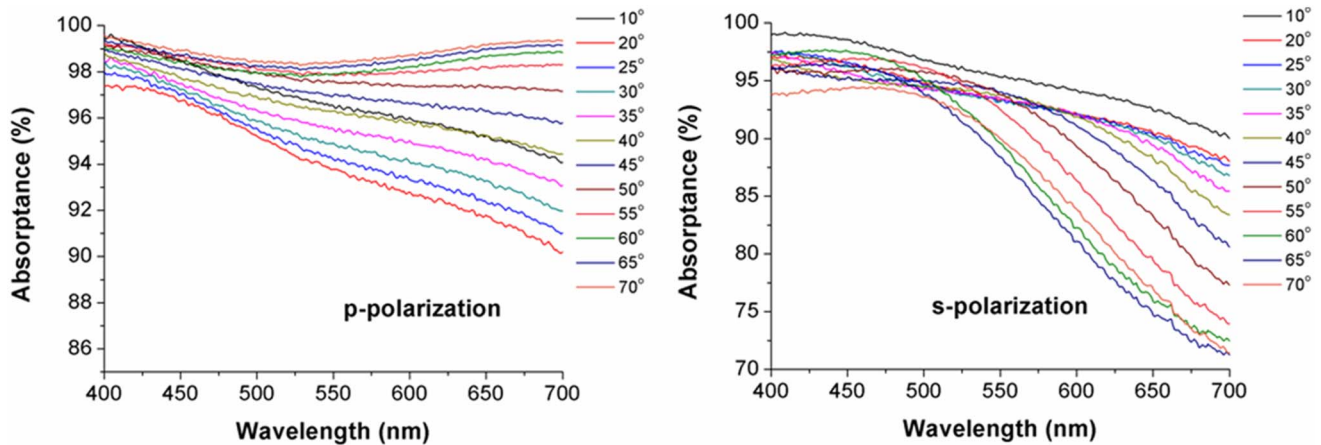


Figure 8 | Left: Two optical images of a silicon wafer either uncoated or coated with the SWF. The uncoated wafer is brightly reflective in contrast with the coated wafer. Right: Measured spectra of the average reflectance  $R = (R_p + R_s)/2$  and the average absorbance  $A = 1 - R$  of the SWF-coated silicon wafer for  $\theta = 5^\circ$ . The inset shows the magnified spectrum of  $R$ .



**Figure 9** | Measured spectra of the absorbances of an SWF-coated silicon wafer, for p- or s-polarized light incident at angle  $\theta \in [20^\circ, 55^\circ]$  with respect to the z axis.

Figure 9 presents plots of the measured absorbances  $A_p = 1 - R_p$  and  $A_s = 1 - R_s$  of the SWF-coated silicon wafer as functions of  $\lambda \in [400, 700]$  nm and  $\theta \in [10^\circ, 70^\circ]$ . For  $\theta \in [20^\circ, 40^\circ]$ , the spectra of  $A_p$  show that this quantity exceeds 90% and has a spectrally averaged value of about 94%. The spectral average of  $A_s$  drops to about 90% for  $\theta \in [10^\circ, 50^\circ]$ , and then to 86% for  $\theta = 70^\circ$ . The spectral average of  $A_p$  is higher than that of  $A_s$  and is in excess of 96% for  $\theta \in [10^\circ, 70^\circ]$ . Thus, broadband absorption is exhibited even for significantly oblique incidence conditions.

**Performance comparison.** In order to evaluate the antireflection performance of the SWF deposited on the amorphous-silicon wafer, we computed the reflectance and absorbance spectra of a silicon wafer coated with a double-layer antireflection (DLAR) coating designed and fabricated by Dhungel *et al.*<sup>19</sup>. This DLAR coating comprises a 61-nm-thick  $\text{SiN}_x$  layer over which a 107-nm-thick  $\text{MgF}_2$  layer is present. As Ref. 19 contains the spectra only for normal incidence ( $\theta = 0^\circ$ ), we computed the spectra for  $\theta \in [0^\circ, 60^\circ]$  with the relative permittivities of silicon and  $\text{MgF}_2$  obtained from

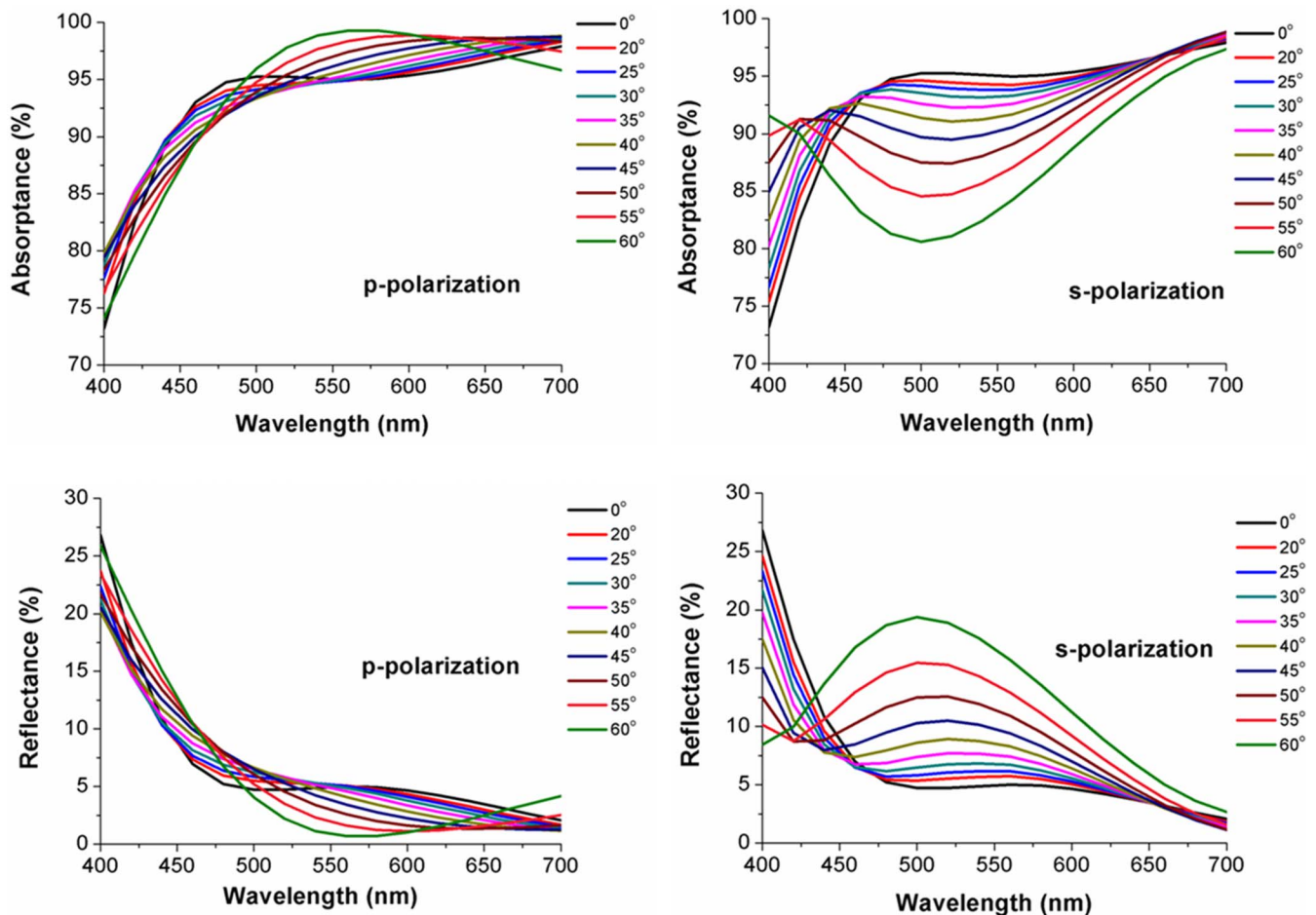


**Figure 10** | Computed spectra of the absorbances and reflectances of a silicon wafer with a  $\text{MgF}_2/\text{SiN}_x$  DLAR coating on top<sup>19</sup>, for p- or s-polarized light incident at angle  $\theta \in [0^\circ, 60^\circ]$  with respect to the z axis.

Macleod Software<sup>20</sup> and the relative permittivity of  $\text{SiN}_x$  adjusted so as to reproduce the reflectance values of Dhungel *et al.*<sup>19</sup> for normal incidence.

The computed spectra for the DLAR-coated silicon wafer are provided in Fig. 10. A comparison of Figs. 8 and 9 shows that the SWF clearly outperforms the DLAR coating<sup>19</sup> in reducing the reflection of *p*-polarized incident light, especially for shorter wavelengths in the visible regime. For *s*-polarized light, the reflection-reduction performances are quite similar.

Another comparison was made with a three-layer antireflection (TLAR) coating designed using a genetic algorithm and deposited on a silicon wafer by Poxson *et al.*<sup>21</sup>. The TLAR coating is 508-nm thick and comprises a  $\text{TiO}_2$  layer sandwiched between two  $\text{SiO}_2$  layers of unequal thickness and unequal porosity, all deposited using the OAD technique. The upper bound of the reflectance of the TLAR-coated silicon wafer for normal incidence and for  $\lambda \in [400, 700]$  nm is 5%<sup>21</sup>, somewhat lower than 6% for the SWF in Fig. 8(b). Using the data provided in Ref. 21, we averaged the polarization-averaged reflectance of the TLAR-coated silicon wafer over  $\theta \in [20^\circ, 55^\circ]$  and  $\lambda \in [400, 700]$  nm and determined that quantity to be 7%. From Fig. 9, the same quantity for the SWF-coated silicon wafer turned out to be 5.8%. A comparison of the spectra of the polarization- and incidence-angle averaged reflectances of a TLAR-coated silicon wafer and an SWF-coated silicon wafer, presented in Fig. 11, also leads to the conclusion that the SWF-coated silicon wafer exhibits comparable antireflection performance—which can be upgraded to better, considering that the TLAR is about 742-nm thick whereas the SWF is just 480-nm thick.

Emulating closely packed arrays of sharply tapered pyramids in microwave anechoic chambers,<sup>22,23</sup> and often said to be inspired<sup>24</sup> by ciliary structures found on the ommatidia of moths and other dipterans, arrays of parallel tapered nanonipples have been shown to have excellent broadband antireflection attributes. Comparison with published data<sup>3</sup> on a 1600-nm-thick array of nanonipples revealed that the SWF yields somewhat poorer performance but it is just 480-nm thick.

## Discussion

We fabricated a thin film comprising randomly distributed nanopillars with a distribution of cross-sectional diameters, each nanopillar a metal/dielectric/metal sandwich. This SWF also has transverse morphological isotropy at macroscopic length scales.

The reflectance of an SWF-coated glass slide for normal incidence was found to be less than 1.05% over the blue-to-red spectral regime. Measurement of the reflection and transmission coefficients in the

blue-to-red regime and subsequent analysis showed that the SWF responds to normal illumination with almost linear dispersion, low extinction coefficient, weakly dispersive forward and backward impedances, and high figure of merit. The SWF has a low extinction coefficient and its phase thickness is close to a *negative* wavelength in the blue-to-red spectral regime, which factors promote destructive interference between reflections originating at the SWF/glass and the air/SWF interfaces. Furthermore, the SWF provides a weakly dispersive impedance match between air and glass. To our knowledge, this is a new modality to achieve broadband reflection reduction.

The reflectance of an SWF-coated silicon wafer for normal incidence was less than 1.35% over the visible regime. Furthermore, broadband reflection-reduction, over a wide range of incidence angles and regardless of the polarization state of the incident light, was observed. The novel antireflection coating is expected to be useful for solar cells, light-emitting devices, and other optical devices.

## Methods

**Fabrication of SWFs.** Two Al/ $\text{SiO}_2$ /Al SWFs with different thicknesses were deposited using the OAD technique. The electron-beam evaporation chamber containing the substrate and the targets of aluminum and silicon dioxide was pumped to a base pressure of  $4 \times 10^{-6}$  Torr prior to evaporation. The target-to-substrate distance was fixed at 25 cm. The collimated vapor flux of either Al or  $\text{SiO}_2$  was directed to towards the substrate at an angle of  $1^\circ$  with respect to the substrate plane. The substrate was made to spin about its central normal axis at an angular speed of 10 rpm, which caused the growing film to comprise upright nanopillars. Either a 3-mm-thick BK7 glass slide or a polished, 0.8-mm-thick, amorphous-silicon wafer was used as the substrate. Monitored by a quartz crystal microbalance, the nominal deposition rate was kept around 1 nm/s. A 210-nm-thick layer of Al was deposited first as the bottom layer, followed by a 45-nm-thick layer of  $\text{SiO}_2$ , and then a 225-nm-thick top layer of Al. Thus, the total thickness *d* of the SWF is 480 nm.

**Optical characterization at normal incidence.** The spectra of the transmittances  $T_j$  and reflectances  $R_j$ ,  $j \in (x, y)$ , were measured on a TRIAX 180 compact imaging spectrometer (Horiba Jobin Yvon) for  $\lambda \in [400, 700]$  nm. For these measurements, the SWF was deposited on a BK7 glass slide.

The complex-valued reflection coefficients  $r_j$  and transmission coefficients  $t_j$ ,  $j \in (x, y)$ , of the same SWF were measured using a walk-off interferometer with a wavelength-tunable 35 KAP 431–220 Ion Laser System (CVI Melles Griot);  $R_j = |r_j|^2$  and  $T_j = N_s |t_j|^2$ , where  $N_s$  is the refractive index of the glass slide. These measurements were carried out at five values of  $\lambda$ : 476, 514, 568, 647, and 676 nm.

**Optical characterization at oblique incidence.** The reflectance of the SWF deposited on an opaque 0.8-mm-thick wafer of amorphous silicon was measured as a function of the angle of incidence  $\theta \in [20^\circ, 55^\circ]$  with respect to the *z* axis, using the TRIAX spectrometer. The incident light could be either *p*- or *s*-polarized.

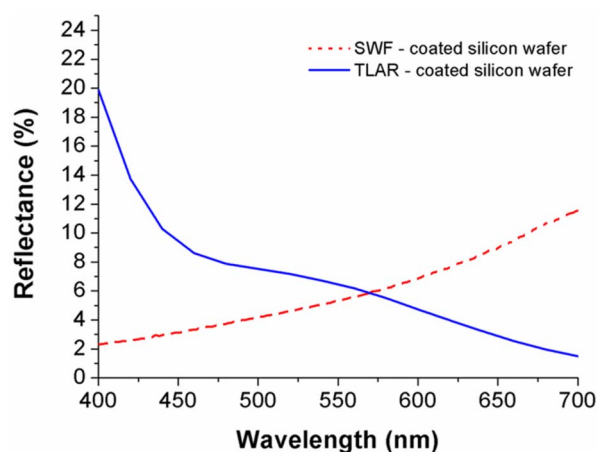


**Figure 11** | Computed spectra of  $R = (R_D + R_S)/2$  averaged over  $\theta \in [20^\circ, 55^\circ]$  for a TLAR-coated silicon wafer<sup>21</sup> and an SWF-coated silicon wafer.

- Macleod, H. A. *Thin-film Optical Filters* (Taylor & Francis, 2000).
- Dobrowolski, J. A., Poitras, D., Ma, P., Vakil, H. & Acree, M. Toward perfect antireflection coatings: numerical investigation. *Appl. Opt.* **41**, 3075–3083 (2002).
- Huang, Y.-F. *et al.* Improved broadband and quasi-omnidirectional antireflection properties with biomimetic silicon nanostructures. *Nature Nanotechnol.* **2**, 770–774 (2007).
- Xi, J.-Q. *et al.* Optical thin-film materials with low refractive index for broadband elimination of Fresnel reflection. *Nature Photon.* **1**, 176–179 (2007).
- Schurig, D. *et al.* Metamaterial electromagnetic cloak at microwave frequencies. *Science* **314**, 977–980 (2006).
- Lu, W. T. & Sridhar, S. Superlens imaging theory for anisotropic nanostructured metamaterials with broadband all-angle negative refraction. *Phys. Rev. B* **77**, 233101 (2008).
- Soukoulis, C. M. & Wegener, M. Past achievements and future challenges in the development of three-dimensional photonic metamaterials. *Nature Photon.* **5**, 523–530 (2011).
- Kriegler, C. E., Rill, M. S., Linden, S. & Wegener, M. Bianisotropic photonic metamaterials. *IEEE J. Sel. Top. Quantum Electron.* **16**, 367–375 (2010).
- Cox, J. T., Hass, G. & Rowntree, R. F. Two-layer anti-reflection coatings for glass in the near infrared. *Vacuum* **4**, 445–455 (1954).
- Jen, Y. J. *et al.* Silver/silicon dioxide/silver sandwich films in the blue-to-red spectral regime with negative-real refractive index. *Appl. Phys. Lett.* **99**, 181117 (2011).
- Güney, D. Ö. & Aslam, M. I. Comment on Silver/silicon dioxide/silver sandwich films in the blue-to-red spectral regime with negative-real refractive index. *Appl. Phys. Lett.* **101**, 156101 (2012).
- Jen, Y.-J. & Lakhtakia, A. Response to Comment on Silver/silicon dioxide/silver sandwich films in the blue-to-red spectral regime with negative-real refractive index. *Appl. Phys. Lett.* **101**, 156102 (2012).



13. Hodgkinson, I. J. & Wu, Q. H. *Birefringent Thin Films and Polarizing Elements* (World Scientific, 1997).
14. Lakhtakia, A. & Messier, R. *Sculptured Thin Films: Nanoengineered Morphology and Optics* (SPIE Press, 2005).
15. Smith, G. B. & Maarouf, A. I. Optical response in nanostructured thin metal films with dielectric over-layers. *Opt. Commun.* **242**, 383–392 (2004).
16. Jen, Y.-J., Lakhtakia, A., Yu, C.-W., & Wang, Y.-H. Negative real parts of the equivalent permittivity, permeability, and refractive index of sculptured-nanorod arrays of silver. *J. Vac. Sci. Technol. A* **28**, 1078–1083 (2010).
17. Xiao, S. *et al.* Loss-free and active optical negative-index metamaterials. *Nature* **466**, 735–738 (2010).
18. Kim, S. Y. & Vedom, K. Analytic solution of the pseudo-Brewster angle. *J. Opt. Soc. Am. A* **3**, 1772–1773 (1986).
19. Dhungel, S. K. *et al.* Double-layer antireflection coating of MgF<sub>2</sub>/SiN<sub>x</sub> for crystalline silicon solar cells. *J. Korean Phys. Soc.* **49**, 885–889 (2006).
20. Optical Thin-Film Software: The Essential Macleod (Thin Film Center Inc., Version 8.18.0), <http://www.thinfilmcenter.com/essential.html> (accessed March 25, 2013).
21. Poxson, D. J., Schubert, M. F., Mont, F. W., Schubert, E. F. & Kim, J. K. Broadband omnidirectional antireflection coatings optimized by genetic algorithm. *Opt. Lett.* **34**, 728–730 (2009).
22. Guy, A. W. Miniature anechoic chamber for chronic exposure of small animals to plane-wave microwave fields. *J. Microw. Power* **14**, 327–338 (1979).
23. Lakhtakia, A. & Iskander, M. F. Theoretical and experimental evaluation of power absorption in elongated biological objects at and beyond resonance. *IEEE Trans. Electromag. Compat.* **25**, 448–453 (1983).
24. Boden, S. A. & Bagnall, D. M. Tunable reflection minima of nanostructured antireflective surfaces. *Appl. Phys. Lett.* **93**, 133108 (2008).

## Acknowledgments

This work was supported by grants from the National Taipei University of Technology, the National Science Council of the Republic of China (NSC 99-2221-E-027-043-MY3 and NSC 101-3113-P-002-021), and the Charles Godfrey Binder Endowment at the Pennsylvania State University.

## Author contributions

Y.J.J. and A.L. co-directed the study and conducted a meta-analysis on all experimental and computational data. M.J.L. constructed the optical set-up and analyzed the data. W.H.W., H.M.W. and H.S.L. fabricated and characterized SWF samples. Y.J.J. and A.L. co-wrote the manuscript.

## Additional information

**Competing financial interests:** The authors declare no competing financial interests.

**License:** This work is licensed under a Creative Commons Attribution-NonCommercial-NoDerivs 3.0 Unported License. To view a copy of this license, visit <http://creativecommons.org/licenses/by-nc-nd/3.0/>

**How to cite this article:** Jen, Y. *et al.* Metal/dielectric/metal sandwich film for broadband reflection reduction. *Sci. Rep.* **3**, 1672; DOI:10.1038/srep01672 (2013).